PUBLICATIONS OF THE ASTRONOMICAL SOCIETY OF THE PACIFIC, **122**:1122–1131, 2010 September

Thickness of the Atmospheric Boundary Layer Above Dome A, Antarctica, during 2009

C. S. BONNER,[1] M. C. B. ASHLEY,[1] X. CUI,[2] L. FENG,[3] X. GONG,[2] J. S. LAWRENCE,[1,4,5] D. M. LUONG-VAN,[1] Z. SHANG,[6] J. W. V. STOREY,[1] L. WANG,[3,7] H. YANG,[8] J. YANG,[3] X. ZHOU,[9] AND Z. ZHU[3]

Received 2010 May 8; accepted 2010 July 7; published 2010 August 5

ABSTRACT. The domes, or local elevation maxima, on the Antarctic plateau provide a unique opportunity for ground-based astronomy in that the turbulent boundary layer is so thin that a telescope on a small tower can be in the free atmosphere, i.e., the portion of the atmosphere in which the turbulence is decoupled from the effect of the Earth's surface. There, it can enjoy a free atmosphere which itself appears to offer superior conditions to that of temperate sites. This breaks the problem of characterizing the turbulence at Antarctic plateau sites into two separate tasks: determining the variability, distribution and thickness of the boundary layer, and characterizing the free atmosphere. In this article we tackle the first of these tasks using a high-resolution, low minimum sample height sonic radar (SODAR) called Snodar that has been specifically designed to characterize the Antarctic boundary thickness and structure. Snodar delivers a vertical resolution of 0.9 m, with a minimum sampling height of 8 m. Snodar sampled the first 180 m of the atmosphere with 0.9 m resolution every 10 s at Dome A, Antarctica between 2009 February 4 and 2009 August 18. The median thickness of the boundary layer over this period was 13.9 m, with the 25th and 75th percentiles at 9.7 m and 19.7 m, respectively. The data collected from Dome A also show that, while the boundary layer can be stable for several hundred hours at a time, it can also be highly variable and must be sampled on the time scale of minutes to properly characterize its thickness.

Online material: color figures

1. INTRODUCTION

Early predictions were made by Harper (1989) and Gillingham (1991) that the high Antarctic plateau might be an excellent location for an astronomical observatory. Marks et al. (1999) used balloon-borne microthermal sensors to profile the optical turbulence over the South Pole and found that the median free-atmosphere seeing was remarkably low, at 0.32″. The seeing from the surface level, however, was degraded to ~1.6″ by a turbulent boundary layer (Marks et al. 1996; Loewenstein et al. 1998). This boundary layer was shown to be 100–300 m thick (Marks et al. 1999; Travouillon et al. 2003).

The atmospheric boundary layer is the lowest region of the atmosphere, and is directly influenced by its proximity to the Earth's surface. It is almost always continuously turbulent over its entire depth (Stull 1988). The atmospheric boundary layer can extend up to several kilometers at temperate sites, but is typically only tens of meters thick over the high Antarctic plateau. A *stable boundary layer* forms when the Earth's surface is cooler than the air above, resulting in a positive vertical temperature gradient. This usually occurs at night, and the strong vertical stratification results in little vertical mixing. In contrast, a *convective boundary layer* forms when the Earth's surface is hotter than the air above it, resulting in a negative vertical temperature gradient; this typically forms during the day. A convective boundary layer is well mixed by convection. A stable boundary layer is separated from the free atmosphere by a *residual layer* and a *capping inversion*. A convective boundary layer is separated from the free atmosphere by an *entrainment zone* (Stull 1988).

The thickness of the boundary layer generally increases as wind speeds within the boundary layer increase. Winds within the boundary layer over Antarctica are usually katabatic in nature. This suggests that local elevation maxima on the Antarctic plateau, such as Dome A and Dome C, could potentially have a much thinner boundary layer than the South Pole, due to their relative lack of katabatic winds (Marks et al. 2002). Dome C is a

[1] School of Physics, University of New South Wales, NSW 2052, Australia; cbonner@phys.unsw.edu.au.
[2] Nanjing Insititute of Astronomical Optics & Technology, Nanjing 210042, China.
[3] Purple Mountain Observatory, Nanjing 210008, China.
[4] Department of Physics, Macquarie University, NSW 2109, Australia.
[5] Anglo-Australian Observatory, NSW 1710, Australia.
[6] Tianjin Normal University, Tianjin 300074, China.
[7] Department of Physics and Astronomy, George P. and Cynthia W. Mitchell Institute for Fundamental Physics and Astronomy, Texas A&M University, College Station, TX 77843.
[8] Polar Research Institute of China, Shanghai 200136, China.
[9] National Astronomical Observatories, Beijing 100012, China.

local elevation maximum at an elevation of 3250 m, and is one of the highest domes on the plateau. Dome A is the highest peak on the Antarctic plateau at an elevation of 4090 m.

Testing of Dome C for its potential as an astronomical observatory began in 1996 (Valenziano & dall'Oglio 1999). Lawrence et al. (2004) showed that the free-atmosphere seeing at Dome C was exceptionally good, with a mean of 0.27″ during 2004 April–May, and that the boundary layer was less than 30 m high. Field campaigns followed with balloon-borne microthermal sensors and DIMMs (Differential Image Motion Monitors) at various heights. Agabi et al. (2006), Trinquet et al. (2008) and Aristidi et al. (2009) reported that the ground level seeing at Dome C was limited by a boundary layer approximately $25 \sim 40$ m high, with a median free-atmosphere seeing of around 0.36″.

Swain & Gallee (2006) used meteorological models of the atmosphere over Antarctica to search for the best sites for astronomy. The seeing and boundary-layer thickness predicted by the simulations were in good agreement with observations made at the South Pole and Dome C. These simulations highlighted Dome A and Dome F as having the lowest boundary layers and close to the best free-atmosphere seeing.

Since the boundary layer above the Antarctic plateau is so thin during winter, it is technically feasible to build a telescope on a tower and access the free-atmosphere seeing (see, e.g., Saunders et al. 2008). Towers of a suitable design have been used for solar astronomy at temperate sites, e.g., Hammerschlag et al. (2006). Site testing for astronomical seeing in Antarctica is thus broken into two separate tasks: determining the height of the required telescope tower by measuring the variability, distribution, and thickness of the boundary layer; and characterizing the residual seeing from the free atmosphere. A high-resolution SODAR and MASS (Multi-Aperture Scintillation Sensor) are close to the optimal pair of instruments to perform these two tasks. A MASS is insensitive to the first 500 m of the atmosphere but reaches all the way from there to the mesosphere, while a SODAR can profile the lowest few hundred meters of the atmosphere. Both of these instruments can be run autonomously and neither requires a tower or elevated platform. A DIMM, which is the traditional instrument for site characterization, is, however, not ideal in Antarctica as it measures the optical parameters integrated over the full height of the atmosphere. Because the vast majority of the turbulence is within the boundary layer, this information is mainly useful if the DIMM is placed completely above the boundary layer or at exactly the same height as that of the future telescope—which is not known in advance.

To conduct our measurements at Dome A, which is currently uninhabited apart from a few weeks during summer each year, we used the PLATeau Observatory (PLATO). PLATO is a self-contained automated observatory designed and built by the University of New South Wales, and provides a platform from which astronomy, site testing, and atmospheric sciences can be conducted year-round at remote sites on the high Antarctic plateau (Lawrence et al. 2008, 2009). PLATO was deployed to Dome A in 2008 January, ran throughout the 2008 winter (Yang et al. 2008), and has been continuously in operation since 2009 January to the time of writing (2010 May).

A high-resolution low minimum sample height sonic radar (SODAR) called Snodar was included in the suite of instruments deployed with PLATO. Snodar was specifically designed to characterize the thickness and structure of the boundary layer on the high Antarctic plateau. Snodar delivers a vertical resolution of 0.9 m and a minimum sampling height of 8 m. Snodar ran at Dome A from 2009 February 4 to 2009 August 18; we present here the results from this period.

We first discuss how acoustic remote sensing can profile optical turbulence, and how the thickness of the boundary layer can then be derived from turbulence profiles.

2. PROFILING OPTICAL TURBULENCE IN ANTARCTICA

The spatial resolution of astronomical images is degraded by perturbations to the wavefront entering an imaging device. The Earth's atmosphere is the primary source of these wavefront perturbations in modern optical astronomy. While adaptive optics (AO) can correct for some wavefront perturbation, builders of large optical telescopes still search for sites with little optical turbulence, as the complexity of AO systems increases rapidly, and the final image quality declines rapidly, with increasing turbulence (Tyson 2000). The wavefront perturbations can be characterized by their spatial coherence (isoplanatic angle, θ_0), temporal coherence (time constant, τ_0), and amplitude (seeing, ϵ_0) in the image plane. These parameters can be calculated for a telescope at a given height above the ground if the optical turbulence, characterized by the refractive index structure function constant, C_N^2, along the optical path is known.

Optical turbulence can be measured either remotely, or in situ, by a variety of means; Storey et al. (2008) give an overview of modern methods and instruments to profile optical turbulence in Antarctica. One of the important challenges is avoiding ice formation on the entrance aperture of the measuring instrument. While this can be done in a straightforward manner by heating the aperture, care must be taken to avoid self-generated turbulence. Instruments that are insensitive to turbulence very close to the instrument are thus at a large advantage. The most common instruments for characterizing optical turbulence during site testing are SODAR, DIMM, MASS and balloon-borne microthermal sensors. Atmospheric modeling is also starting to make an important impact on turbulence forecasting (Lascaux et al. 2009) and on site selection (Swain & Gallee 2006; Saunders et al. 2009).

A SODAR emits an intense, directional pulse of sound into the atmosphere and records the faint backscatter from atmospheric turbulence (further described in § 2.1). SODARs are suitable for profiling turbulence within the first 1 km of the

atmosphere, although they are difficult to calibrate to obtain absolute values of turbulence. See Dragonette et al. (1981), Travouillon (2006), and Bonner et al. (2008) for various calibration methods. A SODAR has constant vertical resolution as a function of height.

A differential image-motion monitor (DIMM) is a simple and robust instrument that measures integrated optical parameters along the line of sight from the instrument to the top of the atmosphere. A DIMM measures the difference in wavefront slope at two points separated by some distance, using the relative motion between two images of the same source (Sarazin & Roddier 1990). A full turbulence profile with height cannot be recovered. However, if multiple DIMMs at different heights are used, as in Aristidi et al. (2009), a coarse measurement of the boundary-layer thickness can be obtained. Such a method requires multiple DIMMs and tower facilities.

A multiaperture scintillation sensor (MASS) uses photon counting on 4 concentric apertures to measure 4 normal and 6 differential scintillation indices (Kornilov et al. 2003). Each of these scintillation indices has a known weighting function, or sensitivity, to turbulence as a function of height, allowing the turbulence to be decomposed into 6 layers. A MASS is insensitive to turbulence within the lowest 500 m of the atmosphere and is well suited to characterizing the free-atmosphere turbulence.

Scintillation detection and ranging (SCIDAR) examines the autocorrelation of the scintillation pattern of a binary star in a telescopes pupil plane to determine the vertical atmospheric turbulence profile with a resolution on the order of 1 km (Rocca et al. 1974). Exposures on the order of milliseconds are required to freeze the scintillation patterns. The cross-correlation of sequential frames can also be examined to determine the horizontal wind speed profile. Similarly to a MASS, a SCIDAR is insensitive to the turbulence in the lower part of the atmosphere. Fuchs et al. (1994) proposed the generalized SCIDAR which examines the autocorrelation in the conjugate plane of the telescopes pupil, that is, the analysis plane is moved to a negative height of several kilometers below the telescope. The generalized SCIDAR then becomes sensitive to turbulence along the entire optical path. A SCIDAR does however require bright binary stars, high-sensitivity high-speed cameras and a meter-class optical telescope.

Balloon-borne microthermal sensors measure in situ temperature differences between two points separated by some distance ρ as the balloon rises from ground level up to $\approx$25 km, where the balloon bursts. The temperature structure function constant C_T^2 can be calculated directly from the differential temperature measurements. Tatarskii (1971) shows that the refractive index and temperature structure function constants are related by

$$C_N^2 = \left[\frac{77.6 \times 10^{-6}}{T^2} P\right]^2 C_T^2,$$

where P is the atmospheric pressure in millibars and T is the temperature in Kelvin. C_N^2 and C_T^2 have dimensions $\mathrm{m}^{-2/3}$ and $\mathrm{K}^2\,\mathrm{m}^{-2/3}$, respectively. Balloon-borne microthermals can therefore generate a calibrated optical turbulence profile. The vertical resolution of this method is limited by the speed of the balloon's ascent to $5 \sim 10$ m.

Microthermal sensors can also be mounted on masts or towers to provide continuous turbulence measurements at fixed heights. Microthermal sensors use extremely delicate fine-wire thermocouples or thermistors to achieve the required frequency response (few hundred Hz). Alternatively, fast sonic anemometers can provide the instantaneous air temperature, which can be used to calculate turbulence. Sonic anemometers are generally robust, but are expensive and difficult to keep ice-free, and are more suitable for permanent installations (Travouillon et al. 2008; Schöck et al. 2009).

2.1. ACOUSTIC TURBULENCE PROFILING

Andrey Kolmogorov's statistical theory of turbulence describes turbulent fields with very high Reynolds numbers and shows that the "inertial" range of a turbulent field can be described by the use of structure functions (Kolmogorov 1980). Kolmogorov's theory is based on the idea that energy enters a turbulent field at some outer scale L_0 and is redistributed by eddy action to smaller and smaller scales until the inner scale l_0 is reached. There, the energy is dissipated as heat by molecular viscosity. l_0 is generally on the scale of millimeters, while L_0 is typically tens of meters and is dependent on the geometry of the turbulent field. Length scales L, where $l_0 \ll L \ll L_0$, are said to be in the inertial range. Tatarskii (1971) shows that electromagnetic and acoustic wave propagation in a turbulent medium results in scattering of the propagating energy and perturbation of the original wavefront. If the turbulent fields obey Kolmogorov's theory, then the acoustic scattering cross-section $\sigma_{\mathrm{scatter}}$ at scattering angle θ of a turbulent field is given by (Tatarskii 1971)

$$\sigma_{\mathrm{scatter}} = 0.03\ \mathrm{k}^{1/3} \cos^2\theta \left(\sin\frac{\theta}{2}\right)^{-11/3} \left[\frac{C_V^2}{c_s^2}\cos^2\frac{\theta}{2} + 0.013\frac{C_T^2}{T^2}\right], \quad (1)$$

where c_s is the speed of sound, k is the wave number of the incident acoustic energy, T is the average temperature, and C_V^2 and C_T^2 are the velocity and temperature structure function constants, respectively. The scattering cross-section is the scattered power per unit volume per incident power per unit area, having dimensions m^{-1}. C_V^2 can be eliminated by setting θ to 2π; this can be achieved by colocating the transmitter and receiver, creating a "monostatic" SODAR. It is reasonably straightforward to show (Little 1969) that the classical radar

equation can be modified for acoustics, and that the operation of an idealized SODAR is given by

$$P_r = P_t \eta \frac{e^{-2\alpha h}}{h^2} \sigma_{\text{scatter}}(h) + P_n,$$

where h is the height of the scattering volume; η is the efficiency, or gain, of the system; α is the atmospheric attenuation coefficient; P_t and P_r are the power transmitted and received, respectively; and P_n is the noise power. The height of the scattering volume can be calculated from the time of flight and the known speed of sound, c_s. If a monostatic SODAR is used, then the received power is proportional to C_T^2 after correcting for atmospheric attenuation and $1/h^2$ spreading. The contributions to seeing, isoplanatic angle, and time constant can then be calculated. The range and sensitivity of a SODAR is limited by atmospheric attenuation, $1/h^2$ spreading, and noise. The minimum sampling height of a SODAR is limited by acoustic reverberation within the antenna structure and electrical ringing within the receiver electronics. The vertical resolution of a vertically pointing monostatic SODAR, dh, is determined by the length τ of the transmitted acoustic pulse and the speed of sound. We have

$$dh = \frac{C_s^{\tau}}{2}.$$

2.2. INSTRUMENT DESCRIPTION

Snodar is a true monostatic high-frequency SODAR designed specifically to profile optical turbulence within the first 180 m of the atmosphere autonomously on the Antarctic plateau. To allow maximum flexibility and robustness, Snodar is largely software defined and can operate at arbitrary frequencies between 3–15 kHz. A USB sound card samples the returned echo with 16 bit resolution at 96 kHz; a PC/104 computer running Debian Linux then performs signal processing in real time. Snodar runs autonomously, storing data on USB flash disks for manual retrieval the following summer. Processed data can be downloaded through the PLATO facility via the Iridium satellite network. Snodar has a minimum sampling height of 8 m and a vertical resolution better than 1 m. The acoustic design of Snodar is given in Bonner et al. (2009a) and an overview of the electrical design is presented in Bonner et al. (2009b).

Snodar has an external antenna structure that can be exposed to temperatures as low as -80°C, and an electronics module that is kept above -20°C inside the PLATO instrument module approximately 15 m from the antenna. A horn-loaded compression driver (JBL2402H) is used as an acoustic transducer and is located near the focal point of a 0.9 m f/0.6 offset parabolic reflector. The transducer and reflector are housed inside an acoustically insulated 1.6 m tall sound cone to suppress fixed echoes and ambient noise. Heaters are installed on the back of the reflector to inhibit the formation of frost; small amounts of snow can also be sublimed with the heaters. A low-noise solid-state switch and impedance matching network are installed near the transducer.

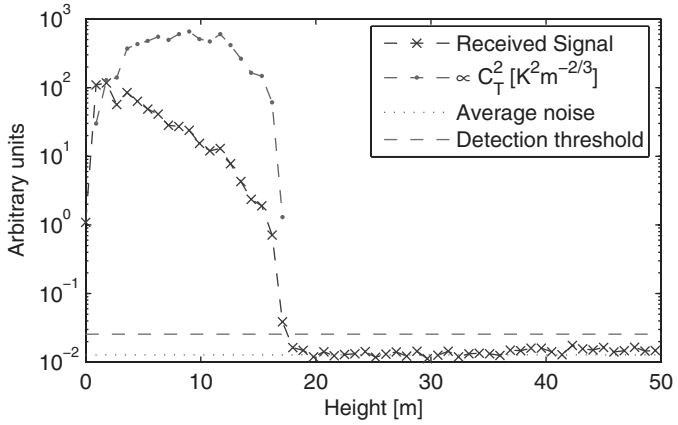

FIG. 1.—30 minute integration from Dome A at 2009 April 9 01:00 UTC. The signal strength is in arbitrary units as intensity is yet to be calibrated. The received signal is saturated at $\approx 10^2$ until a height of 2 m, then the ringing decays exponentially until it reaches the noise floor of $\approx 10^{-2}$ at 8 m. The signal from acoustic backscatter starts to become greater than the ringing at 4 m. The derived value of C_T^2 is seen to drop 2 orders of magnitude between 15 m and 17 m. The signal is no longer significantly statistically different from the noise above 18 m. See the electronic edition of the *PASP* for a color version of this figure.

Snodar uses a unique in situ calibration method to measure the system gain (Bonner et al. 2008). In situ calibration allows the time-varying attenuation caused by snow on the parabolic reflector to be corrected. Calibration pulses were taken every 30 minutes during 2009.

The dominant error in the thickness of the boundary layer determined by Snodar is the uncertainty in the air temperature. Due to a lack of accurate temperature measurements at Dome A during this observation period, a constant temperature of -60°C is used for the analysis presented here. This assumption introduces less than $\pm 5\%$ error in the height and spatial resolution, provided that the actual air temperature is between -80°C and -40°C.

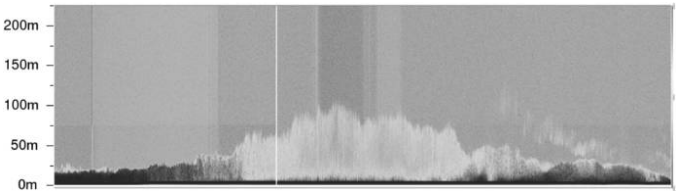

FIG. 2.—Facsimile plot from 2010 February 9 21:00 UTC to 2010 February 10 21:00 UTC at Dome A. The boundary layer does not exceed 110 m in thickness over this period. See the electronic edition of the *PASP* for a color version of this figure.

3. OBSERVATIONS

Snodar started collecting data at Dome A on 2009 February 4. Good data were obtained until 2009 August 18, after which time the top of the boundary layer increased and its maximum extent could no longer be observed as snow accumulation in the parabolic reflector reduced the signal-to-noise ratio (S/N). Data quality for the whole period was assessed manually and was deemed good when the top of the boundary layer could be identified by a rapid transition from a turbulent to a stable atmosphere.

Acoustic pulses 6 ms in length with frequencies of 4, 5, and 6 kHz were used to profile the turbulence to a vertical resolution of 0.9 m to a height of 180 m, every 10 s. Multiple frequencies were used to verify that the turbulence followed a Kolmogorov power law and that equation (1) was followed.

At Dome A, the extremely low free-atmosphere turbulence is below Snodar's sensitivity at even a few meters above the

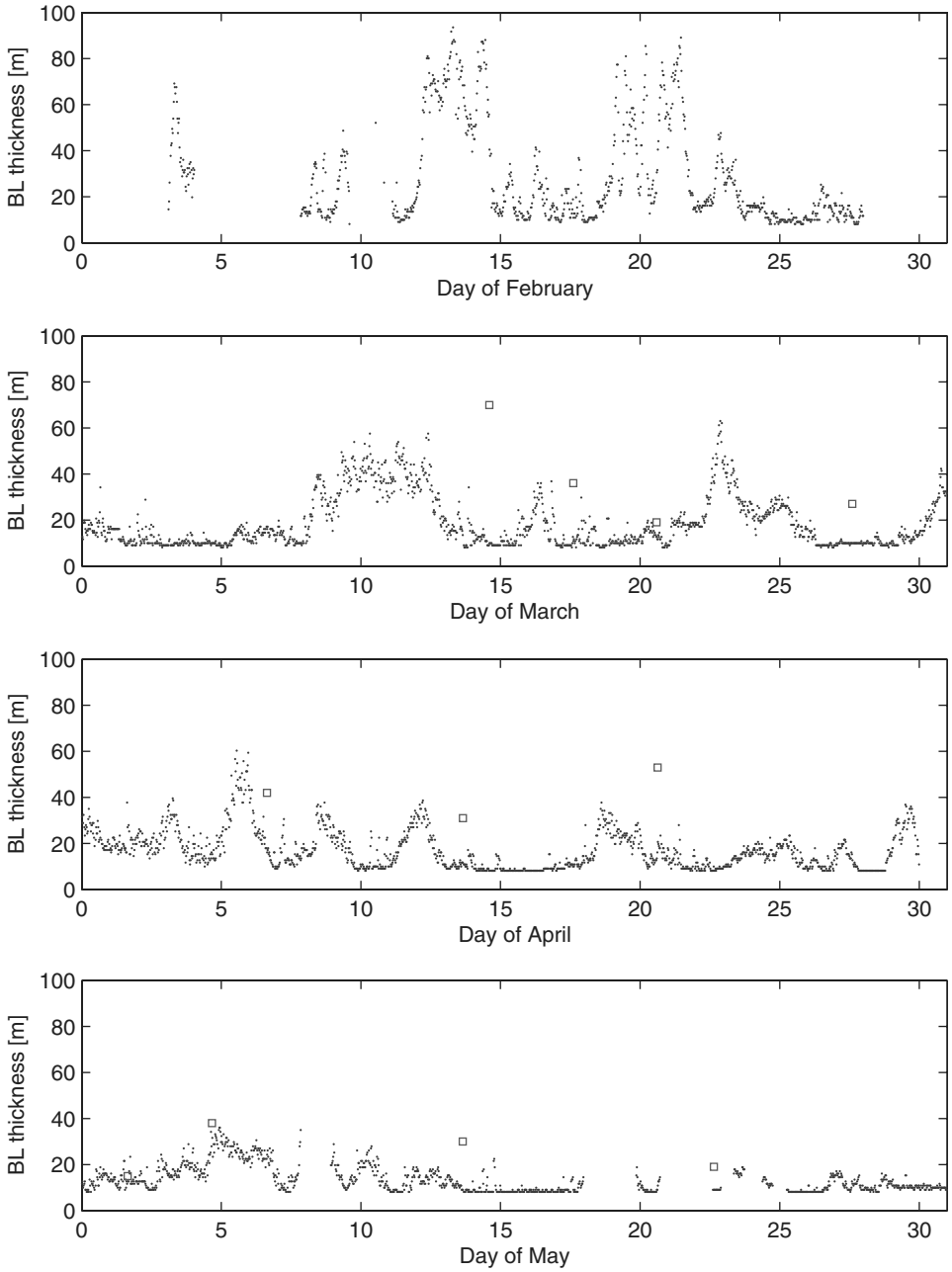

FIG. 3.—Boundary-layer height at Dome A from 2009 February to 2009 May with 30 minute averages. *Open squares* indicate the boundary-layer thickness at Dome C on the same day of the year, but during 2005, from Trinquet et al. (2008). See the electronic edition of the *PASP* for a color version of this figure.

boundary layer. Figure 1 is a 30 minute average of the optical turbulence profile from Dome A at 2009 April 9 01:00 UTC—note that in this plot C_T^2 is uncalibrated and given in arbitrary units as the calibration pulse data from 2009 are not yet available and further work is required to calibrate the instrument. This is a typical example of the winter boundary layer at Dome A where the optical turbulence drops several orders of magnitude within a few meters. Previous studies of the winter boundary layer on the high Antarctic plateau lacked the spatial resolution to observe this rapid transition from turbulent to the free atmosphere, although observers at Dome C have reported that the top of the boundary layer can be so sharp that it appears as a horizontal line when viewed from the window of the elevated station (Fossat, E. 1980, private communication).

In the absence of data sensitive to this sharp transition, previous workers such as Trinquet et al. (2008) defined the boundary-layer thickness as the height above 8 m that contains 90% of the turbulence within the lowest 1 km of the atmosphere. Unfortunately, this definition can lead to both underestimates and overestimates of the true thickness. For example, in Figure 1, if the turbulence remains below 10^{-2} arbitrary units from 17 m to the top of the atmosphere, then the lowest 17 m will contain $\approx 99.5\%$ of the total turbulence within the lowest 1 km of the atmosphere; in this case, the 90% definition will underestimate the height at which a telescope should be placed to be above the boundary layer by 10%. Conversely, if there is significant turbulence in the free atmosphere up to 1 km, then the 90% definition can lead to a thickness that is considerably above the true boundary layer; however, in practice this condition does not appear to occur on the Antarctic plateau.

The fundamental issue is that the definition of the thickness of the boundary layer should be independent of any turbulence in the rest of the atmosphere.

It is advantageous to use a definition of the thickness of the boundary layer that can be applied to calibrated and uncalibrated turbulence profiles, gives a height at which a telescope

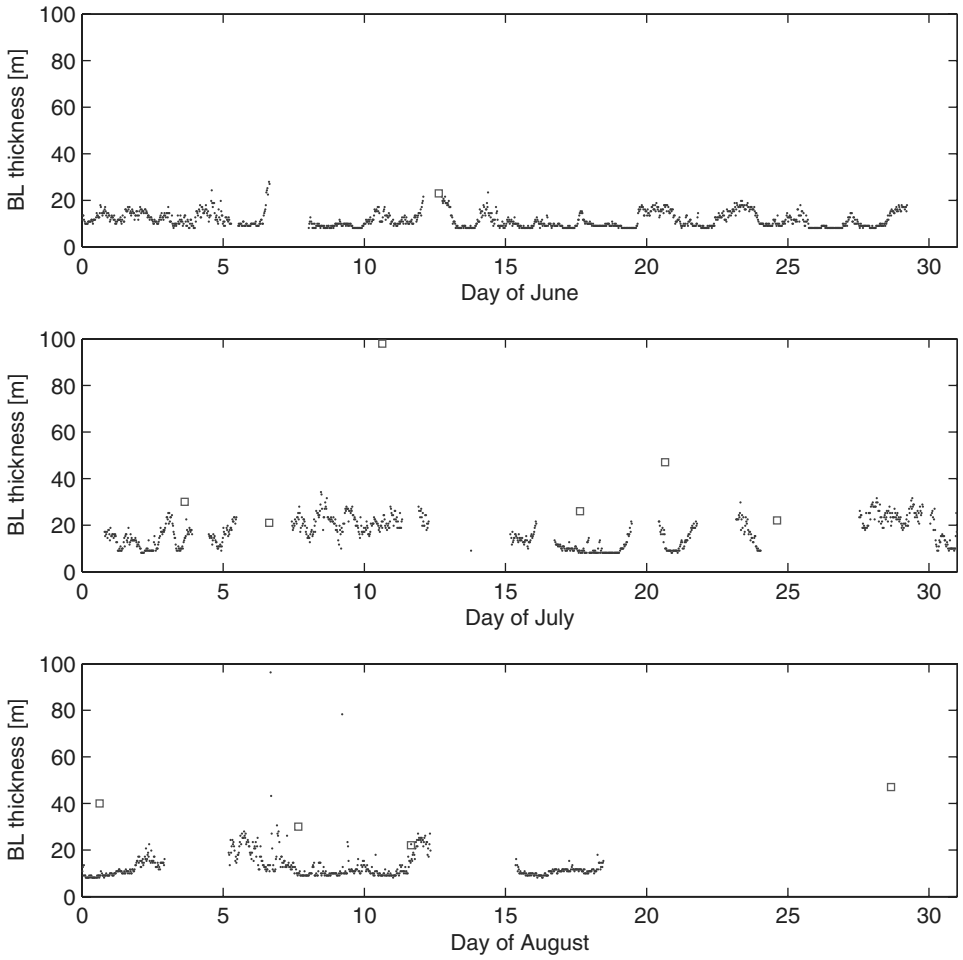

FIG. 4.—Boundary-layer height at Dome A from 2009 June to 2009 August with 30 minute averages. *Open squares* indicate the boundary-layer thickness at Dome C on the same day of the year, but during 2005, from Trinquet et al. (2008). See the electronic edition of the *PASP* for a color version of this figure.

should be located, and provides a useful mixing height for boundary-layer meteorology. To this end, we have adapted the definitions used by Swain & Gallee (2006) and Stull (1988). Our adopted definition is as follows: *The thickness of the boundary layer is where C_T^2 or equivalently, C_N^2, first reduces to 1% of its original value.*

This definition is reasonably insensitive to the details of the measurements within the boundary layer because of the rapid transition from turbulence to calm atmosphere on the high Antarctic plateau (provided the first data point is within the boundary layer). Because the turbulence within the boundary layer varies by only a factor of a few (see Fig. 1), the exact position of the initial data point is of little importance. Such a ratiometric definition does, however, increase the effective minimum sampling height by one range-bin. This means the minimum detectable boundary-layer thickness for Snodar is 9 m. The boundary-layer thickness is 17.1 m $\pm$ 1 m for the data shown in Figure 1.

The summer boundary layer observed at Dome A is remarkably similar to that observed at Dome C by Mastrantonio et al.

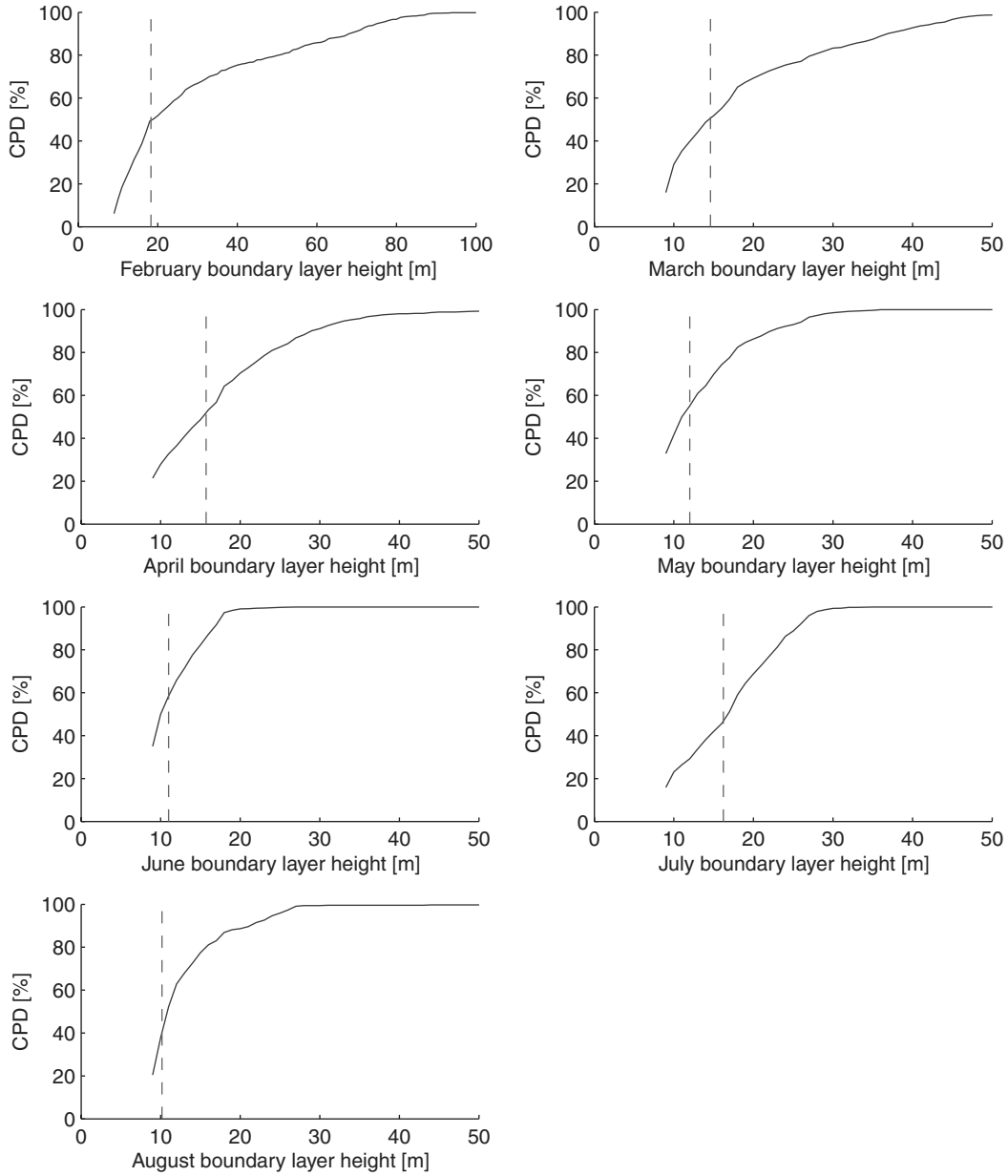

FIG. 5.—Cumulative probability distribution of the boundary-layer thickness at Dome A from 2009 February to 2009 August with 30 minute averages. Note the change in horizontal axis for February. See the electronic edition of the *PASP* for a color version of this figure.

TABLE 1
BOUNDARY-LAYER THICKNESS STATISTICS FOR EACH MONTH IN 2009 (ERROR IS ±5%)

Month	Data availability	Number of 30 minute averages[a]	25th Percentile	50th Percentile	75th Percentile
Feb	70.10%	942	12.4 m	18.3 m	39.6 m
Mar	100%	1488	9.3 m	14.6 m	23.3 m
Apr	99.90%	1439	9.4 m	15.7 m	21.2 m
May	79.40%	1181	<9 m	12.0 m	16.8 m
Jun	90.00%	1296	<9 m	11.0 m	13.4 m
Jul	56.90%	846	10.4 m	16.2 m	21.5 m
Aug	42.70%	635	9.7 m	10.2 m	14.5 m
Entire period (Feb–Aug)	77.00%	7827	9.7 m	13.9 m	19.7 m

[a] 25th percentile, 50th percentile, and 75th percentile.

(1999). A facsimile plot from 2010 February 9 21:00 UTC to 2010 February 10 21:00 UTC at Dome A is shown in Figure 2. The boundary layer shows a strong diurnal variation but does not exceed 110 m in height over this period. The horizontal band at the bottom of the plot is an artifact caused by transducer ringing.

3.1. RESULTS

Our data were averaged into 30 minute blocks. Monthly time series of the boundary-layer thickness are shown in Figures 3 and 4. Monthly cumulative probability distributions of the boundary-layer thickness are shown in Figure 5. Table 1 shows the monthly data availability; number of 30 minute averages; and 25th, 50th and 75th percentiles. Data availability was reduced in July and August as a result of snow accumulation within Snodar's antenna. This decreased the S/N to a point where the top of the boundary layer could not be identified as a rapid drop in C_T^2. For each month, the available data from Dome C (Trinquet et al. 2008) for the corresponding month in 2005 are also plotted. Obviously, there should be no correlation between these data sets. However, assuming that the boundary layer at Dome C is as variable as it is at Dome A, these plots do illustrate the difficulty of extracting meaningful statistics from sparsely sampled data. Figure 6 shows the cumulative probability distributions of the boundary layer at Dome A during 2009 and at Dome C during 2005. The median boundary-layer thickness from the field campaigns are 13.9 m and 33 m, respectively.

A diurnal variation is apparent during 2009 February; however, it does not appear to be the primary driver of the thickness of the boundary layer. No significant diurnal variation or significant periodicity is seen in the other months. While the thickness of the boundary layer is highly variable throughout the entire year, there are also periods where it is constant for several days.

PLATO is equipped with several webcameras, one of which points toward the engine module that houses diesel generators for power generation. Under certain illumination and wind conditions, the exhaust from the engines can give information on the behavior of the boundary layer. There are three occasions where there was little wind and the boundary layer was below the minimum sampling height of Snodar. In the first, the exhaust plume from the engine module was confined and appeared to be trapped in stratified air at a height of 5 m at 2009 April 10 22:00 UTC. From the plume behavior and the absence of any turbulence detected by Snodar, we can infer that the boundary layer was stable during this period, with a thickness between 5 m and 8 m.

The second, and perhaps the most interesting, event occurred at 2009 April 29 09:00 UTC. The exhaust plume fell to the snow surface after leaving the exhaust pipe and gradually dispersed. There was little wind at this time and no turbulence was detected by Snodar. The exhaust plume generally disperses with vertical symmetry when it does not interact with a solid surface or temperature inversion. A vertical asymmetry is introduced when the exhaust plume interacts with a boundary where mixing can not take place. Such a boundary may be a temperature inversion or a solid surface; the exhaust plume will disperse parallel to the

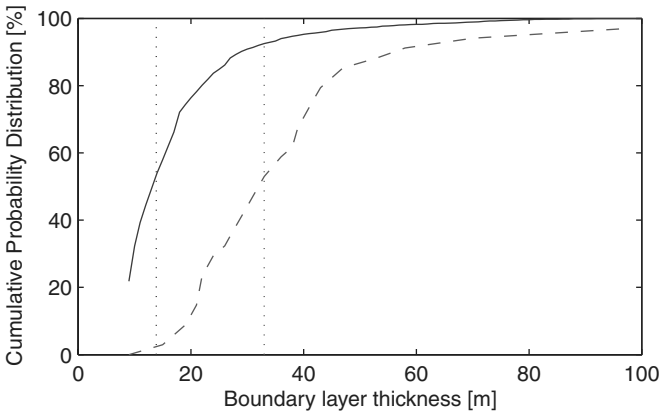

FIG. 6.—Cumulative probability distributions of the boundary-layer thickness over Dome A during 2009 (*solid line*), and Dome C during 2005 (*dashed line*). Data for Dome C are from Trinquet et al. (2008). Median boundary-layer thickness for Dome A and Dome C is 13.9 m and 33 m, respectively. See the electronic edition of the *PASP* for a color version of this figure.

boundary in such circumstances.

The third event occurred at 2009 June 17 12:56 UTC. The exhaust plume appeared to settle on top of a temperature inversion approximately 5 m above the ground at this time. From this we can infer that the boundary-layer thickness was approximately 5 m. A similar circumstance was observed at 2009 April 29 08:00 UTC, or 1 hr preceding the second event.

These three observations give support to the conclusion of Swain & Gallee (2006) that the boundary layer could at times be as thin as a few meters.

The high spatial and temporal resolution of Snodar has also revealed great complexity within the boundary layer itself. Gravity, or buoyancy, waves can be observed within the boundary layer along with complex layered structures.

4. DISCUSSION AND CONCLUSIONS

The thickness of the atmospheric boundary layer above Dome A has been studied with a high-resolution low minimum sampling height SODAR called Snodar. The first 180 m of the atmosphere was profiled with 0.9 m resolution every 10 s from 2009 February 4 to 2009 August 18 with 77% data availability. The median thickness of the boundary layer was 13.9 m, with the 25th and 75th percentiles at 9.7 m and 19.7 m, respectively. This is considerably lower than the height of the boundary layer at Dome C during 2005 where the median thickness was 33 m, with the 25th and 75th percentiles at 25 m and 42 m, respectively (Trinquet et al. 2008). The data collected from Dome A show that while the boundary layer can be stable for several hundred hours, it can also be highly variable and must be sampled on the time scale of minutes to properly characterize its height.

It is possible that the large difference between the reported boundary-layer heights at Dome A and Dome C is due not only to the differences in the locations, but also to the different methods and definitions used by the different campaigns. To resolve these issues, it would be highly desirable to simultaneously operate Snodars at Dome C, Dome F, Dome A, and other Antarctic plateau locations to allow direct comparisons of the sites.

Snodar has a unique calibration method that allows the calibrated turbulence profiles to be obtained. The data files with these calibration pulses are too large for retrieval via Iridium and must be physically returned by the annual traverse. Once these data are available, it will be possible to calculate the *intensity* of the boundary-layer turbulence, and hence, the boundary-layer contribution to seeing. Further site-testing work is ongoing at Dome A to assess sky brightness, cloud coverage, auroral activity, wind speed, and atmospheric transmission. A MASS is planned to be installed in future years to characterize the free atmosphere. Snodar was serviced again in 2010 January and is still collecting data at the time of submission of this article.

The authors wish to thank all members of the 2008, 2009, and 2010 Polar Research Institute of China Dome A expedition for their heroic effort in reaching the site and for the invaluable assistance they provided to the expedition astronomers in setting up the PLATO observatory and the Snodar instruments. This research is financially supported by the Australian Research Council, the Australian Antarctic Division, the Chinese Academy of Sciences, the National Natural Science Foundation of China, the US National Science Foundation, and the US Antarctic Program.

REFERENCES

Agabi, A., Aristidi, E., Azouit, M., Fossat, E., Martin, F., Sadibekova, T., Vernin, J., & Ziad, A. 2006, PASP, 118, 344

Aristidi, E., Fossat, E., & Agabi, A. 2009, A&A, 499, 955

Bonner, C. S., Ashley, M. C. B., Lawrence, J. S., Storey, J. W. V., Luong-Van, D. M., & Bradley, S. G. 2008, Proc. SPIE, 7014, 70146I

Bonner, C. S., Ashley, M. C. B., Lawrence, J. S., Luong-Van, D. M., & Storey, J. W. V. 2009a, Acoustics Australia, 37, 47

Bonner, C. S., Ashley, M. C. B., Lawrence, J. S., Luong-Van, D. M., & Storey, J. W. V. 2009b, Proc. International Conf. Optical Turbulence, Astronomy meets Meteorology, ed. E. Masciadri, & M. Sarazin (London: Imperial College Press World Scientific), 264

Dragonette, L. R., Numrich, S. K., & Frank, L. J. 1981, Acoust. Soc. Am, 69, 1186

Fuchs, A., Tallon, M., & Vernin, J. 1994, Proc. SPIE, 2222, 682

Gillingham, P. R. 1991, Proc. Astron. Soc. Australia, 9, 55

Hammerschlag, R. H., Bettonvil, F. C. M., & Jaegers, A. P. L. 2006, Proc. SPIE, 6273, 627310

Harper, D. A. 1989, AIP Conf. Proc. 198, 123

Kolmogorov, A. N. 1980, Proc. R. Soc. London, Ser A., 434, 9

Kornilov, V., et al. 2003, Proc. SPIE, 4839, 837

Lascaux, F., Masciadri, E., Hagelin, S., & Stoesz, J. 2009, MNRAS, 398, 1093

Lawrence, J. S., Ashley, M. C. B., Tokovinin, A., & Travouillon, T. 2004, Nature, 431, 278

Lawrence, J. S., et al. 2008, Proc. SPIE, 7012, 701227

———. 2009, Rev. Sci. Inst, 80, 064501

Little, C. G. 1969, Proc. IEEE, 57, 571

Loewenstein, R. F., Bero, C., Lloyd, J. P., Mrozek, F., Bally, J., & Theil, D. 1998, ASP Conf. Ser. 141, Astrophysics from Antarctica, ed. G. Novak, & R. Landsberg (San Francisco: ASP), 296

Marks, R. D., Vernin, J., Azouit, M., Briggs, J. W., Burton, M. G., Ashley, M. C. B., & Manigault, J. F. 1996, A&A, 118, 385

Marks, R. D., Vernin, J., Azouit, M., Manigault, J. F., & Cleelin, C. 1999, A&AS, 134, 161

Marks, R. D. 2002, A&A, 385, 328

Mastrantonio, G., Malvestuto, V., Argentini, S., Georgiadis, T., & Viola, A. 1999, Meteorol. Atmospheric Phys., 71, 127

Rocca, A., Roddier, F., & Vernin, J. 1974, J. Opt. Soc. Am. A, 64, 1000

Sarazin, M., & Roddier, F. 1990, A&A, 227, 294

Saunders, W., Gillingham, P. R., McGrath, A. J., Storey, J. W. V., & Lawrence, J. S. 2008, EAS Publ. Ser. 33, Proc. 2nd ARENA Conf., ed. H. Zinnecker, H. Rauer, & N. Epchtein, 285
Saunders, W., Lawrence, J. S., Storey, J. W. V., Ashley, M. C. B., Kato, S., Minnis, P., Winker, D., Liu, G., et al. 2009, PASP, 121, 976
Schöck, M., Els, S., Riddle, R., Skidmore, W., Travouillon, T., Blum, R., Bustos, E., Chanan, G., et al. 2009, PASP, 121, 384
Storey, J. W. V., Ashley, M. C. B., & Lawrence, J. S. 2009, Proc. International Conf. Optical Turbulence, Astronomy meets Meteorology, ed. Masciadri, E., & Sarazin, M. (London: Imperial College Press World Scientific), 82
Stull, R. B. 1988, An Introduction to Boundary Layer Meteorology (Dordrecht: Kluwer)
Swain, M. R., & Gallee, H. 2006, PASP, 118, 1190
Tatarskii, V. I. 1971, The Effects of the Turbulent Atmosphere on Wave Propagation (Jerusalem: Keter Press)
Travouillon, T., Ashley, M. C. B., Burton, M. G., Storey, J. W. V., & Loewenstein, R. F. 2003, A&A, 400, 1163
Travouillon, T. 2006, Proc. SPIE, 6267, 626720
Travouillon, T., Aristidi, E., Fossat, E., Lawrence, J. S., Mekarnia, D., Moore, A., Skidmore, W., & Storey, J. W. V. 2008, Proc. SPIE, 7012, 70124B1
Trinquet, H., Agabi, A., Vernin, J., Azouit, M., Aristidi, E., & Fossat, E. 2008, PASP, 120, 203
Tyson, R. K. 2000, Introduction to Adaptive Optics (Bellingham, WA: SPIE Press)
Valenziano, L., & dall'Oglio, G. 1999, PASA, 16, 167
Yang, H., et al. 2008, PASP, 121, 174